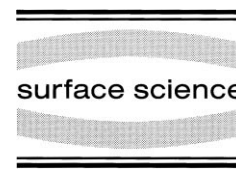




ELSEVIER

Surface Science 465 (2000) 90–96



www.elsevier.nl/locate/susc

Ag films on GaAs(110): dewetting and void growth

M.M.R. Evans, B.Y. Han, J.H. Weaver *

Department of Materials Science and Chemical Engineering University of Minnesota, Minneapolis, MN 55455, USA

Received 8 February 2000; accepted for publication 19 June 2000

Abstract

Scanning tunneling microscopy studies show that atomically flat but slightly corrugated films of Ag(111) can be produced by depositing ~ 15 Å of Ag on GaAs(110) at 40 K and then annealing at 300 K. These films are six layers thick, but they also contain voids that extend to the GaAs surface. Time-dependent imaging shows void growth due to spontaneous dewetting. Void growth is accompanied by the transfer of Ag atoms onto the terraces where elongated, single-height Ag islands formed, with patterns reflecting the corrugation of the Ag film. These results demonstrate that these films are thermodynamically unstable, and they reveal void growth and geometry for a multilayer film. © 2000 Elsevier Science B.V. All rights reserved.

Keywords: Adhesion; Crystallization; Epitaxy; Gallium arsenide; Growth; Scanning tunneling microscopy; Silver; Surface structure, morphology, roughness, and topography; Wetting

1. Introduction

The Ag/GaAs(110) system has attracted interest because atomically flat films can be produced if Ag is vapor-deposited at low temperature and then annealed at room temperature [1]. Low-temperature deposition produces a configuration that is far from equilibrium with Ag covering the GaAs(110) surface, and warming facilitates diffusion, crystal growth, and planarization. This planar structure differs from that achieved by Ag deposition at room temperature where the surface is decorated by multilayer islands having tent-like appearances and specific orientations [2] and different from the surfactant-induced layer by layer growth of Ag/Ag(111) [3]. Zhang et al. [4] have

argued that planar films are stabilized by an electronic contribution to the total energy, an effect that compensates for the unfavorable overlayer–substrate interface energy. They concluded that a six-layer film had an optimized electronic contribution. The experimental studies of Smith et al. [1] showed that depositing somewhat less than 15 Å of Ag resulted in films that were six layers thick but with voids that extended to the GaAs(110) surface. If somewhat more Ag was deposited, then additional layers formed. Further studies of Ag overlayers grown on (110) surfaces of III–V compound semiconductors have shown [5] that Ag on InP(110) forms voids that are longer and thinner than those found by growth on GaAs(110).

This paper examines the stability of Ag films on GaAs(110) to determine whether they represent equilibrium structures or metastable intermediate structures. If the former, then they would not change with time. If the latter, then the films would be unstable, possibly against dewetting. Dewetting

* Permanent address: Department of Materials Science and Engineering, University of Illinois at Urbana-Champaign, Urbana, Illinois, 61801, USA. Fax: +1-217-333-2736.

E-mail address: jweaver@uiuc.edu (J.H. Weaver)

would be reflected by the growth of voids whose origins could be traced to the initial planarization of the film. It would be difficult on perfect or void-free terraces because the energy barrier associated with creation of a critical size void would be large. Void growth would reduce the Ag–GaAs interface area, but it would increase the film thickness and the total length associated with voids and adlayer islands.

Using scanning tunneling microscopy (STM), we have studied the structural evolution as a function of time of samples having a nominal coverage of 15 Å. Initial imaging revealed the distribution and structure of small voids, and successive imaging demonstrated that the voids grew over the course of hours at room temperature. These voids expanded in directions dictated by the symmetry of the fcc Ag(111) structure and the Ag–GaAs interface. Void expansion delivered Ag atoms to the terraces and single-height islands developed along GaAs[1 $\bar{1}$ 0] with widths that were integer multiples of 15.4 Å, a characteristic dimension that reflected strain due to accommodation of Ag rows. This void expansion and subsequent overlayer growth shows that the magic-layer structure is an intermediate configuration, not a globally optimized configuration.

2. Experiment

The experiments were performed in a two-chamber vacuum system where the base pressure was 3×10^{-11} Torr. The measurement chamber was equipped with a Park VP.1 STM that operated at room temperature. The attached chamber had capabilities for physical vapor deposition onto samples held at low temperature. Clean GaAs(110) surfaces were prepared by cleaving $4 \times 4 \times 10$ mm³ posts (Zn-doped at 1×10^{18} cm⁻³). Silver was evaporated from resistively heated tungsten boats, and deposition rates were 0.5–1.5 Å min⁻¹, as calibrated with a quartz crystal monitor placed near the sample. The pressure during deposition was $< 3 \times 10^{-10}$ Torr, and a quadrupole mass spectrometer was used to monitor residual gases.

Procedurally, samples were cleaved, inspected visually, and imaged with STM to a verify high

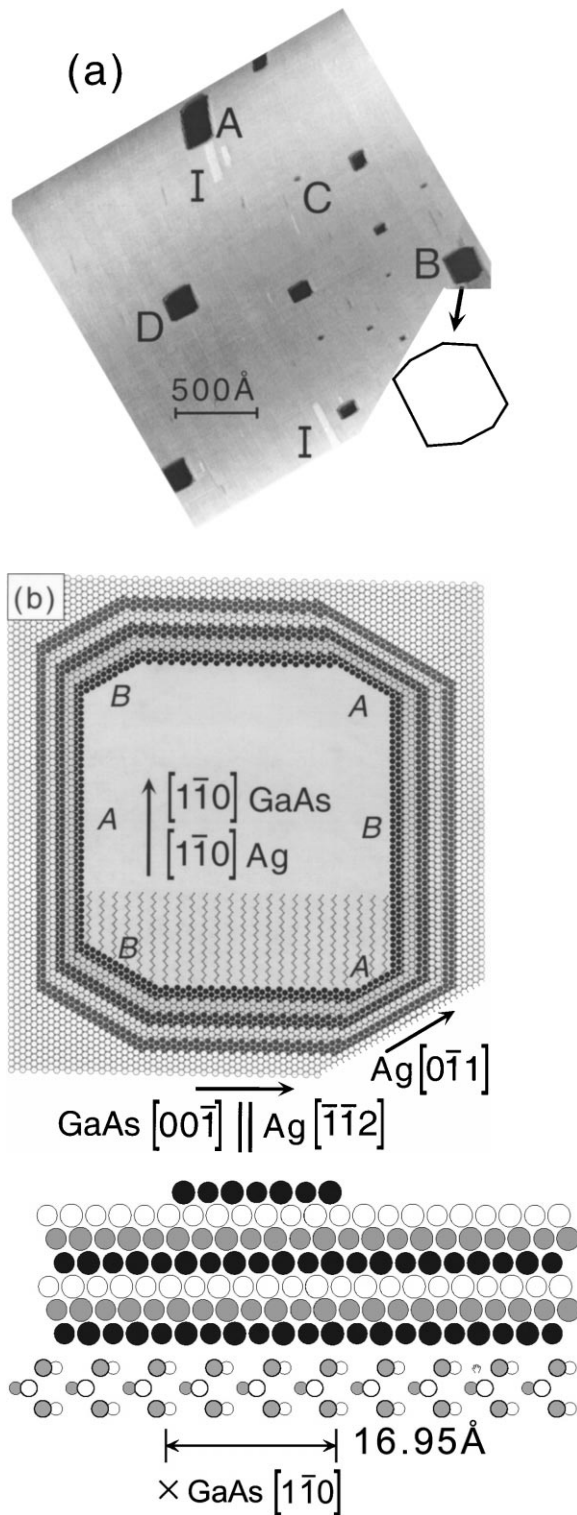
surface quality with terraces extending over thousands of angstroms. They were then transferred to the deposition chamber and placed on a cold stage that was attached via a copper braid to a closed cycle helium refrigerator. Deposition was done after the samples were cooled to ~ 40 K. Immediately after deposition, the refrigerator compressor was turned off, and the warm-up process was started. While this produced a small pressure burst due to H₂ and CO desorption, the ion and turbomolecular pumps kept the pressure below $\sim 4 \times 10^{-10}$ Torr, and recovery into the 10^{-11} Torr range occurred within 1 min. Typically, the samples warmed to ~ 120 K over the course of 2 h and were then transferred to the STM for imaging.

3. Results and discussion

3.1. Film structure

Fig. 1 shows an image that was obtained approximately 4 h after a sample was transferred to the STM. The image is not corrected for thermal drift. Voids in the film are clearly evident, and their projected area deduced from many images is about 2% of the surface. This film is six layers or 15 Å thick, as verified by line scans that crossed voids and imaged the GaAs(110) surface. These voids grew with time, as discussed below, and growth is accompanied by the formation of elongated single-layer thick islands of Ag. These islands are labeled I in Fig. 1a and, since they are near voids, they could have formed during the initial 4 h of aging. Occasionally, there were height variations of ~ 2 Å on the Ag terraces that indicated a buried GaAs step, running along [1 $\bar{1}$ 0]. Higher-resolution images of the Ag terraces revealed stripes due to a height modulation of 0.5–1 Å. They have an average separation of 15.4 Å, and they run parallel to GaAs[1 $\bar{1}$ 0]. Ebert et al. [6] studied these corrugations in detail and showed that the spacing between stripes could be divided into two groups, with a short separation of 12 ± 2 Å and a long separation of 17 ± 2 Å.

The voids of Fig. 1a have sides that are parallel to GaAs [00 $\bar{1}$] and [1 $\bar{1}$ 0], corresponding to Ag[$\bar{1}\bar{1}2$] and Ag[1 $\bar{1}$ 0], respectively. Small voids



like void C, which measured 60 Å \times 50 Å, tend to be rectangular and elongated along GaAs $[00\bar{1}]$. Larger voids like A and B tend to be elongated along GaAs $[\bar{1}\bar{1}0]$. Large voids also tend to have additional sides oriented at 30° from $[00\bar{1}]$, as depicted beneath the image of Fig. 1a for void B (whose rectangular dimensions were 190 Å \times 210 Å). All of these voids extended to the GaAs(110) surface. Smaller voids were also detected, but probing their boundaries and their depth could not be done reliably. These structures differ from the hexagonal single layer islands and holes that can be produced on Ag(111) [7,8].

Fig. 1b shows a proposed geometric structure of void B, a typical void produced by aging. Six layers of fcc Ag(111) are drawn, and the crystallographic faces are defined, giving the symmetry of the Ag film and the termination of the ends of the voids. For fcc Ag(111), there are two distinct structures for the $\langle 10\bar{1} \rangle$ family of steps. The *A* steps have (100) microfacets associated with them, as depicted in Fig. 1b, while *B* steps have (111) microfacets [9]. Both of these steps have linear densities of unity along $\langle 10\bar{1} \rangle$, and the atoms have four nearest in-plane neighbors. In contrast, atoms in the Ag $[\bar{1}\bar{1}2]$ steps have a reduced linear density and only three nearest neighbors. The voids grow along $[\bar{1}\bar{1}0]$, and the details of the step are important for their stability and the transfer of Ag atoms onto the terrace (discussed below).

Fig. 1. (a) STM image of a 15 Å Ag film on GaAs(110). The film is flat but with a regular corrugation of ~ 0.5 Å that runs along GaAs $[\bar{1}\bar{1}0]$. Clearly evident are voids, labelled A–D, and additional Ag on the terrace in the form of islands, I, that elongated along GaAs $[\bar{1}\bar{1}0]$. Void B measures approximately 190 Å \times 210 Å, and its projected shape is indicated. The image is not corrected for drift. (b) Model of void B showing six layers of Ag(111) with six *A*- and *B*-type steps with maximum linear density and $\langle 011 \rangle$ orientations. The two top and bottom boundaries are perpendicular to GaAs $[\bar{1}\bar{1}0]$. The angles formed by the *A*- and *B*-type steps are 26° , as determined by cross-sectional scans. This indicates that the terraces are two atoms in width. Note that imaging to provide the detail of the model was not possible and that Ag atoms at the steps are dynamic at 300 K. The base of the void reveals zigzag rows of GaAs. (c) (bottom figure) Cross-sectional model of the Ag–GaAs interface with GaAs $[\bar{1}\bar{1}0]$ projected into the page. Perspective for Ag is implied by the sizes of the circles denoting Ag atoms, and shading of the Ag overlayer is used to indicate the ABC stacking.

The angles corresponding to the steps in Fig. 1b were determined from line scans that extended from the flat Ag terrace to the base of the void for a large number of voids, including those where the corners were better developed than for void B. We also changed the scan direction and averaged over the six *A*- and *B*-type steps for a given void. Measurement by connecting the 10–90% points on a cross-section gave an angle of $26 \pm 4^\circ$ relative to the Ag(111) terrace. Tip-broadening effects, though not completely eliminated, were not expected to introduce significant errors since the slopes were relatively modest, and the voids were large. Based on these angles and the structure of fcc Ag, an observer would see an average angle of 29.5° at *A*-types steps, 22° at *B*-type steps, and 22.2° at Ag[$\bar{1}\bar{1}2$] steps. While Fig. 1b is drawn to scale with these angles in mind, it is only a guide. Atomic scale details of the angles or step structure could not be resolved at 300 K.

The interface suggested by Fig. 1b for Ag(111) and GaAs(110) does not offer a good lattice match because these surfaces have very different planar densities (1.38×10^{15} vs. 8.85×10^{14} atom cm^{-2} , respectively). Fig. 1c depicts the interface in cross-section where the zigzag rows in Fig. 1b now extend into the page. These rows are 5.65 Å apart, and the row separation for Ag along [$\bar{1}\bar{1}2$] is 2.5 Å. Along [$\bar{1}\bar{1}0$], the Ag spacing is 2.89 Å, and the As–As (or Ga–Ga) spacing is 3.997 Å, giving a period of nearly 84 Å. Six layers of Ag are depicted, separated by 2.36 Å, with the depth perspective for a given plane given by the variations in size. They range in gray scale to draw attention to the A–B–C stacking for fcc [111]. An island of about 17 Å width is included on the terrace. It would have a linear density of unity along [$\bar{1}\bar{1}0$], as do the steps in Fig. 1b. From simple geometric considerations, one can envision the long and the short separations for the modulations reported by Ebert et al. [6] to reflect patterns established by seven Ag atoms overlying three rows of GaAs and five Ag atoms overlying two rows of GaAs. Distortion to optimize interface bonding and atom registry along [$\bar{1}\bar{1}2$] would introduce strain and could account for the 0.5 Å corrugation. This strain could also be responsible for the stability of the voids along GaAs [$\bar{1}\bar{1}0$].

Previous studies by Trafas et al. [2] considered interfaces produced by atom deposition at room temperature. They found hut-like structures with Ag (111) surfaces inclined at about 25° and ($\bar{1}\bar{1}\bar{1}$) inclined at 45° relative to the GaAs surface. The short dimension of the base was parallel to GaAs[00 $\bar{1}$] and the long dimension along [$\bar{1}\bar{1}0$]. They deduced that contact with GaAs was made with Ag(110) planes that were tilted by 10° . Hence, four units of Ag would correspond to three of GaAs along [00 $\bar{1}$]. The planar films investigated here share the alignment along [$\bar{1}\bar{1}0$], and although our films are flat and lack the registry displayed by the huts, it is clear that the interface is strongly biased to favor an atomic registry along the GaAs rows.

3.2. Void growth and coalescence

Fig. 2 provides an $8300 \text{ \AA} \times 10\,000 \text{ \AA}$ overview of the changes associated with multilayer void growth over ~ 170 h, starting from the surface represented by Fig. 1a. Void growth is driven by energetic considerations, but it is slow at room temperature and can be followed with STM. Whereas the projected area of the voids was 2% in Fig. 1a, it now represents 24% of the surface area in Fig. 2. The maximum projected void size initially was $\sim 20\,000 \text{ \AA}^2$ (average 6000 \AA^2), and it increased to $2 \times 10^6 \text{ \AA}^2$ (average $1 \times 10^5 \text{ \AA}^2$). For comparison, void E in Fig. 2 is about the same size as void A in Fig. 1a. Void F is the largest in the image, and it has grown by extended coalescence, as could be seen through time-lapse imaging. Coalescence accounts for the decrease in void density from 4.5 to $2.25 \times 10^{10} \text{ cm}^{-2}$. From Fig. 2, void F is in the process of completing a corner-to-corner merge of two large voids. The exposed GaAs(110) surface also has a step within void F, but it cannot be seen with the gray scale of the figure. Void G shows an end-to-end coalescence process underway involving voids of different widths (growth along [$\bar{1}\bar{1}0$]). Within voids H and J, there are residual multilayer islands of Ag that were isolated from the surrounding terrace by side-by-side void coalescence growth along [00 $\bar{1}$], as will be discussed in the context of Fig. 3. It is important to note that there was no evidence of void generation, consistent with the high barrier

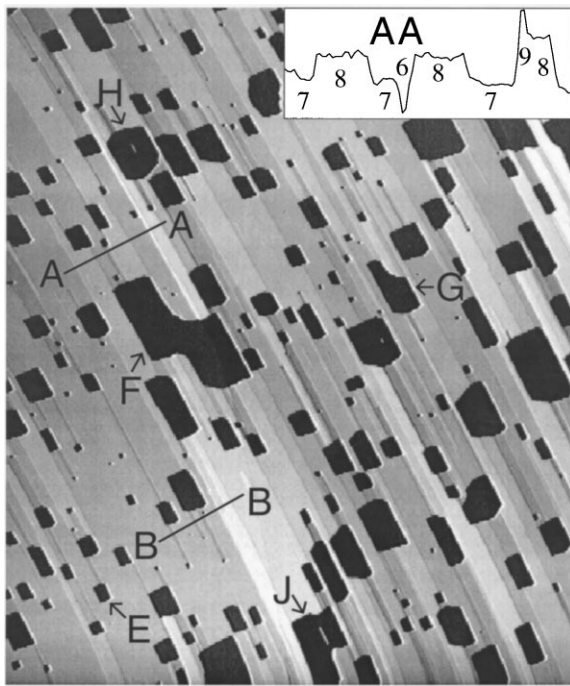


Fig. 2. Large-scale STM image for Ag–GaAs showing dewetting and void coalescence after 170 h. Void growth occurs when Ag atoms are transferred to the terrace, and the result is a thickening of the film. Linescan AA in the inset shows the thickness variation in units of Ag layers. These islands are elongated along GaAs because of the corrugation in the film introduced by the lattice mismatch at the interface, as shown in Fig. 1c. Voids H and J contain strips of residual Ag that were isolated by void coalescence. $8300 \text{ \AA} \times 10000 \text{ \AA}$.

for nucleation of a multilayer void. Instead, all growth is associated with voids whose origin could be traced to the initial planarization process and the shortage of Ag to completely cover the surface.

Fig. 2 shows that Ag atoms expelled during void growth have formed new layers with long single-height steps parallel to GaAs[$\bar{1}\bar{1}0$]. These steps add to the energy of this new configuration, the new layers reduce the electronic energy stabilization described by Zhang et al. [4], but dewetting is driven by an overall lowering in energy. Note that equilibrium island growth can be assumed because adatom redistribution is slow and that the new steps are parallel to the film corrugation. The number of monolayer-equivalents of additional Ag can be estimated by assuming that the voids have vertical walls and that the adatoms are distributed

on the remaining 76% of the surface, giving $0.24 \times 6 \text{ layers} / 0.76 = 1.9$ monolayers (which overestimates because of the vertical wall approximation). In Fig. 2, linescans reveal variations in the film thickness, as in the inset. Line AA crosses areas that are (from left to right) seven, eight, seven, six, eight, seven, nine, and eight layers in thickness. Likewise, line BB crosses areas that are (from left to right) seven, six, seven, six, seven, six, seven, eight, nine, and eight layers thick. From Fig. 2, the six layer terraces that persist are terminated at voids, as can be seen by inspecting the left segment of line BB or the center of line AA.

Fig. 3 focuses on void coalescence and the development of adlayers near them. The images in Fig. 3a–c were acquired 94, 108, and 114 h after warm-up. The starting image shows two large voids, K and L, with sharply defined boundaries, as in Fig. 1b. They are separated by a terrace stripe that is $\sim 90 \text{ \AA}$ wide at its top. Linescans that cross the voids indicate that the surrounding terraces are primarily seven layers thick. Linescan A in Fig. 3a highlights the cross-section of a six-layer segment bounded by a void along the GaAs[$\bar{1}\bar{1}0$] and single height steps along GaAs[$00\bar{1}$], as evident in the line trace at lower right. Fourteen hours later, voids K and L had reduced their total multilayer step length by forming two necks while isolating a residual island within the void. Continued coalescence to Fig. 3c involved considerable material removal along [$\bar{1}\bar{1}0$] in regions where kink densities would be high. There was very little growth along [$00\bar{1}$] or in regions of low kink density established by prior aging. While voids M and N were approximately the same distance from K in Fig. 3a, a neck was established along [$\bar{1}\bar{1}0$] from K to M, but not along [$00\bar{1}$] toward N.

From these growth patterns, we can speculate that A- and B-type Ag< $10\bar{1}$ > multilayer step structures that extend along GaAs[$\bar{1}\bar{1}0$], depicted in Fig. 1b, are the most stable. The prevalence of similar < $10\bar{1}$ > structures at the corners indicates their stability as well, though their formation increases the total step length. We find no voids with hexagonal symmetry. Instead, the more open steps of [$\bar{1}\bar{1}2$] are always observed. Void growth occurs via material removal from these steps, and we expect that the kink formation energy will be

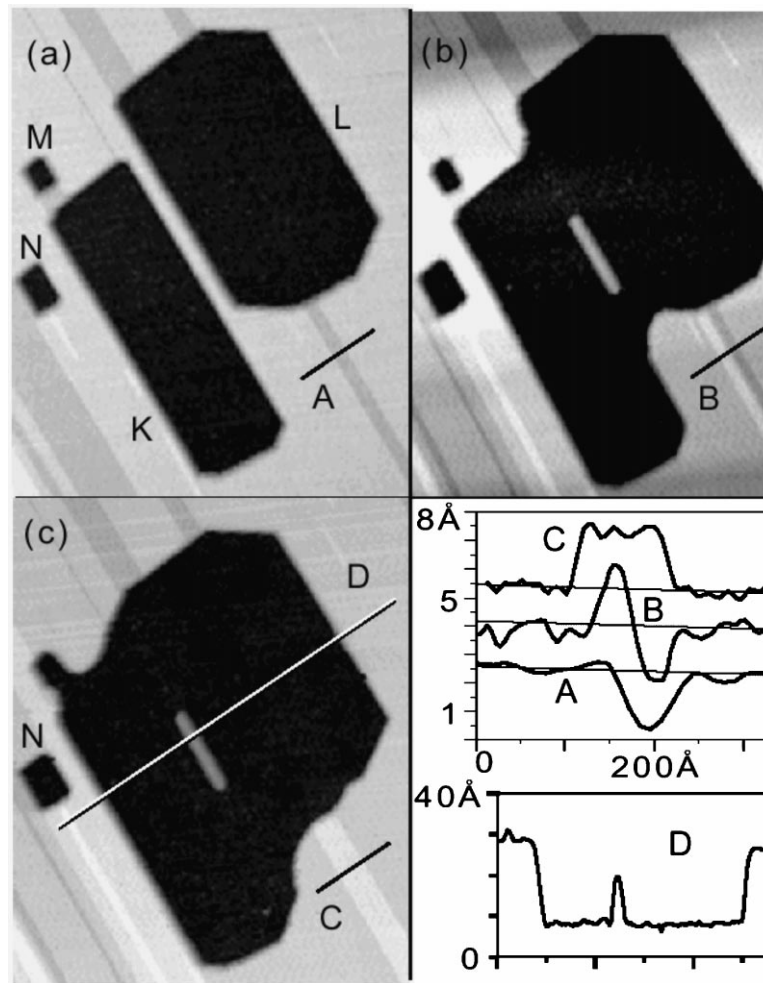


Fig. 3. (a–c) Coalescence of voids K, L, and M. Cross-sections A, B, and C summarize the filling in of the seventh Ag layer and the creation of an eighth. Line scan D displays the cross-section of the large void created by coalescence of K and L, with the residual Ag island isolated from the surround Ag layers. The images were acquired 94, 108, and 114 h after the film was warmed to room temperature. $1550 \text{ \AA} \times 1925 \text{ \AA}$.

less than for the close-packed steps *A* and *B* because of the lower atom coordination. Silver expulsion continues at the irregular edges of the growing voids as high-energy Ag steps evolve into lower-energy structures of *A*- and *B*-type.

Long-lived islands can be created within a void, as in Fig. 3, when necks form at both ends of a terrace stripe. Neck growth occurs by thinning of the Ag multilayer until the GaAs substrate is exposed. Thereafter, an isolated island can shrink only if atoms dissociate from it and diffuse across

GaAs(110) to reach the void edges. The barrier for dissociation should approach the cohesive energy of Ag (2.95 eV), and this accounts for the longevity of the Ag islands. In Fig. 3c, the island is five layers in height, as determined from the linescan, and approximately 25 Ag rows wide at its base.

Inspection of the growth features on the six-layer terraces demonstrates the importance of the corrugation of the Ag film. Linescan A for Fig. 3a reveals a six-layer stripe that is $\sim 100 \text{ \AA}$ wide, bordered on each side by seven layers of Ag. This

width corresponds to approximately seven periods of the 15.4 Å corrugation (which represents the average of short and long separations discussed by Ebert et al. [6]). Linescan B for the same region of Fig. 3b shows that the six-layer region has been reduced to three periods, and adjacent to it, there is an eight-layer elongated island of four periods. By Fig. 3c, the six-layer region has disappeared, and the eight-layer island has a width of nine periods (140 Å).

The importance of the corrugation with regard to island growth can be seen in Fig. 3a, where there is an eight-layer island that is two periods in width and has formed below void N. This island grows away from the void (parallel to GaAs[110]). The limiting factor for lateral expansion of an island would be nucleation of a new stripe of 15.4 Å. Evidence for such growth can be found in this island in Fig. 3c because its width changes from 32 to 48 Å, i.e. from two to three periods. Though the film corrugation is small, it has a profound effect on the evolution of the overlayer.

The coverage tolerance for creating a smooth Ag film was tight. If the amount was too little, then the film would have a greater fraction of voids. If the amount was too much, then adlayers of Ag would form on the 15 Å layer. These adlayers were less elongated than those emphasized here. This can be explained by noting that the degree of supersaturation of Ag atoms was much higher following planarization of an over-grown film than that achieved by room-temperature aging. Hence, it was more likely that the seed of a 15.4 Å increment could be established.

Prior studies of Ag grown at low temperature on GaAs(110) have focused on its tendency to form a highly ordered overlayer of exactly six layers in thickness. They have also dealt with the novel corrugation that is observed and the corrugation pattern, and with the tendency of Ag to form planar overlayers on III–V semiconductor surfaces. They argued that a key component behind film stabilization lay in the electronic confinement between a vacuum and a substrate with a bandgap. This quantum effect had not been included in prior considerations of growth structures based on the balance of bulk energies, surface energies, and interface energies. Here, we have confirmed that

the Ag–GaAs(110) system forms a six-layer film, but we have also shown that it is metastable against spontaneous dewetting and thickening. Accordingly, the planarization associated with warming a low-temperature grown overlayer produces a state that is not the equilibrium configuration. Dewetting that exposes the GaAs surface occurs by mass transport up a series of steps and onto the surface where redistribution gives rise to elongated islands having widths of integer multiples of 15.4 Å. We have argued that this width is the average of that seen by Ebert et al. [6], and we have suggested that it reflects the atomic periodicity of five or seven atoms of Ag trying to accommodate between two or three rows of GaAs(110). Strain is then incorporated into the film and propagated to the surface. Voids produced by dewetting are shown to coalesce following preferred expansion along GaAs[110]||Ag[110]. The patterns can be understood in terms of the atomic structure of the interface and the film symmetry. The void coarsening observed here differs from the inverse process of island coarsening in that we expect minimal Ag exchange between voids and no net capture of diffusing Ag atoms by voids.

Acknowledgement

This work was supported by the US Army Research Office.

References

- [1] A.R. Smith, K.-J. Chao, Q. Niu, C.-K. Shih, *Science* 273 (1996) 226.
- [2] B.M. Trafas, Y.-N. Yang, R.L. Siefert, J.H. Weaver, *Phys. Rev. B* 43 (1991) 14107.
- [3] J. Vrijmoeth, H.A.v.d. Vegt, J.A. Meyer, E. Vlieg, R.J. Behm, *Phys. Rev. Lett.* 72 (1994) 3843.
- [4] Z. Zhang, Q. Niu, C.-K. Shih, *Phys. Rev. Lett.* 80 (1998) 5381.
- [5] K.-J. Chao, Z. Zhang, P. Ebert, C.K. Shih, *Phys. Rev. B* 60 (1999) 4988.
- [6] P. Ebert, K.-J. Chao, Q. Niu, C.K. Shih, *Phys. Rev. Lett.* 83 (1999) 3222.
- [7] J. Li, W.-D. Schneider, *Phys. Rev. Lett.* 80 (1998) 3332.
- [8] S.J. Chey, L. Huang, J.H. Weaver, *Surf. Sci.* 419 (1999) L100.
- [9] R. Ferrando, G. Tréglia, *Phys. Rev. B* 50 (1994) 12104.